Study on Vapor−Liquid Equilibria and Surface Tensions for Nonpolar Fluids by Renormalization Group Theory and Density Gradient Theory

Dong Fu*

School of Environmental Science and Engineering, North China Electric Power University, Baoding, 071003 People's Republic of China

Received: May 31, 2006; In Final Form: July 17, 2006

An equation of state (EOS) applicable for both the uniform and nonuniform fluids is established by using the density-gradient theory (DGT). In the bulk phases, the EOS reduces to statistical associating fluid theory (SAFT). By combining the EOS with the renormalization group theory (RGT), the vapor−liquid-phase equilibria and surface tensions for 10 nonpolar chainlike fluids are investigated from low temperature up to the critical point. The obtained results agree well with the experimental data.

1. Introduction

The vapor−liquid phase equilibrium and the surface tension of fluids play important roles in the development, design, and simulation of many industrial processes, such as chemical engineering and environmental protection. In the recent years, interest increased rapidly in establishing a thermodynamic framework under which both the phase equilibria and interfacial properties can be investigated within a single set of molecular parameters. Although this framework has been tested with success for fluids below the critical region, its application inside the critical region is still challenging.[1−3]

There are two theories popularly used for the investigation of critical properties. One is the renormalization-group theory (RGT)[4−15] and the other is the crossover theory.[16−23] Both the two theories yield good critical properties compared with the experimental data because the long-wavelength density fluctuation is correctly taken into account. However, the classical equation of state, e.g., the SAFT EOS,[24,25] fails to describe the critical properties because the long-wavelength density fluctuation is ignored.

For the formulation of the Helmholtz free energy functional for nonuniform fluids in vapor−liquid surface, there are two theories popularly used. One is the density functional theory (DFT)[26−32] and the other is the density gradient theory (DGT).[33−37] Both of the two theories can be reduced to classical EOS (e.g., SAFT[24,25]) in the bulk phases and correctly capture the qualitative features of the dependence of the interfacial properties as functions of temperature in surface. The main difference between these two theories is that in DGT, there is an additional influence parameter that should be obtained by fitting to the experimental data of surface tensions but in DFT the influence parameter can be obtained by the use of direct correlation function. In general, DFT is theoretically better than DGT because it only needs the molecular parameters regressed from experimental data of bulk phases. However, as the Euler−Lagrange equations must be numerically solved using standard Picard method, the combination of DFT with RGT is very difficult. Compared with DFT, the DGT approach determines the equilibrium density profile from Cahn−Hilliard theory[33] without iteration. Due to its computational convenience, DGT is relatively easier to be combined with RGT for interfacial properties inside the critical region.

The main purpose of this work is to develop an approach that accurately describes both the phase equilibria and surface tensions from low temperature up to the critical region. The DGT is used to formulate the Helmholtz free energy functional. The molecular parameters and the influence parameter are regressed by utilizing the EOS and the experimental data of both phase equilibria and surface tensions below the critical region. The phase equilibria and the surface tensions inside the critical region are improved by RGT.[4−15] The proposed approach is applied to 10 nonpolar chainlike fluids satisfactorily.

2. Theory

2.1. Density Gradient Theory. Cahn and Hilliard[33] proposed that, for a system with two equilibrium phases separated by an interface, the Helmholtz free energy density could be described by expanding in a Taylor series. The expansion is expressed as

$$f[\rho(\mathbf{r})] = f_0[\rho(\mathbf{r})] + \kappa_1[\nabla\rho(\mathbf{r})]^2 + \kappa_2\nabla^2\rho(\mathbf{r}) + \ldots\ldots \quad (1)$$

where $\rho(\mathbf{r})$ is the local number density of molecules at position $\mathbf{r}$ and $f_0[\rho(\mathbf{r})]$ is the free energy density of the uniform state without the interface.

Keeping the two lowest order terms in the expansion, the Helmholtz free energy can be expressed as

$$A[\rho(\mathbf{r})] = \int\{f_0[\rho(\mathbf{r})] + \kappa[\rho(\mathbf{r}),T][\nabla\rho(\mathbf{r})]^2\}\,\mathrm{d}\mathbf{r} \quad (2)$$

where $\kappa[\rho(\mathbf{r}),T]$ is the influence parameter. In principle, $\kappa[\rho(\mathbf{r}),T]$ is dependent on the local density $\rho(\mathbf{r})$ and temperature T. For spherical molecules, it can be expressed as

$$\kappa[\rho(\mathbf{r}),T] = \frac{kT}{6}\int r^2 c[\mathbf{r},\rho(\mathbf{r})]\,\mathrm{d}\mathbf{r} \quad (3)$$

where $c[\mathbf{r},\rho(\mathbf{r})]$ stands for the direct correlation function.

For the vapor−liquid and liquid−liquid surfaces with small density gradients, Cahn and Hilliard[33] proposed that $\kappa[\rho(\mathbf{r}),T]$

* To whom correspondence should be addressed. E-mail: fudong@tsinghua.org.cn.

10.1021/jp063361v CCC: $33.50
Published on Web 09/02/2006

can be expressed as a function of temperature or treated as a constant. By abbreviating $\kappa[\rho(\mathbf{r}),T]$ as κ and replacing $\rho(r)$ with $\rho(z)$, the density gradient $d\rho(z)/dz$ for a vapor−liquid surface is expressed as[33]

$$\frac{d\rho(z)}{dz} = \sqrt{\frac{\Delta f[\rho(z)]}{\kappa}} \tag{4}$$

where

$$\Delta f[\rho(z)] = \kappa\left[\frac{d\rho(z)}{dz}\right]^2$$

is expressed as[33]

$$\Delta f[\rho(z)] = f_0[\rho(z)] - \rho(z)\mu + p \tag{5}$$

where μ and p are the chemical potential and pressure for bulk phases.

The equilibrium density profile $\rho(z)$ is as follows:

$$z = z_0 + \int_{\rho^V}^{\rho^L} \sqrt{\frac{\kappa}{\Delta f[\rho(z)]}}\, d\rho(z) \tag{6}$$

where $\rho(z_0) = (\rho^V + \rho^L)/2$, ρ^V and ρ^L are equilibrium densities for vapor and liquid phases, respectively. By evaluating the integral numerically, a distance z may be determined for any $\rho(z)$ lying between the bulk densities.

Once the equilibrium density profile is obtained, the surface tension can be calculated from[33]

$$\gamma = 2\int_{\rho^V}^{\rho^L} \sqrt{\Delta f[\rho(z)]\kappa}\, d\rho(z) \tag{7}$$

2.2. EOS for the Bulk Phase. In the bulk phase, the Helmholtz free energy for nonpolar fluid can be expressed by SAFT[24,25]

$$\frac{A}{NkT} = \frac{A^{id}}{NkT} + \frac{A^{hs}}{NkT} + \frac{A^{LJ}}{NkT} + \frac{A^{chain}}{NkT} \tag{8}$$

where N is the number of molecules. A^{id} is the free energy of ideal gas in the identical temperature and density. A^{hs}, A^{LJ}, and A^{chain} are the contributions due to hard sphere repulsion, attractive interaction, and the formation of chains, respectively.

A^{id} is given as

$$\frac{A^{id}}{NkT} = \ln(\rho\Lambda^3) - 1 \tag{9}$$

where Λ is de-Broglie thermal wavelength.

A^{hs} can be expressed by the Carnahan−Starling equation[38]

$$\frac{A^{hs}}{NkT} = m\frac{4\eta - 3\eta^2}{(1-\eta)^2} \tag{10}$$

where m is the number of segments, $\eta = \pi/6\, m\rho d^3$ is the packing factor, d is the hard-sphere diameter for each segment. The relationship between d and σ, the soft-sphere diameter, can be expressed as[39]

$$\frac{d}{\sigma} = \frac{1 + 0.2977kT/\epsilon}{1 + 0.33163kT/\epsilon + 0.001047(kT/\epsilon)^2} \tag{11}$$

where ϵ/k is the energy parameter.

A^{LJ} is expressed as[39]

$$\frac{A^{LJ}}{NkT} = m\frac{1}{T_r}\left(A_1^{LJ} + \frac{1}{T_r}A_2^{LJ}\right) \tag{12}$$

where $Tr = kT/\epsilon$ and

$$A_1^{LJ} = \rho_r(-8.5859 - 4.5424\rho_r - 2.1268\rho_r^2 + 10.285\rho_r^3) \tag{13}$$

$$A_2^{LJ} = \rho_r(-1.9075 + 9.9724\rho_r - 22.216\rho_r^2 + 15.904\rho_r^3) \tag{14}$$

where $\rho_r = [6/\sqrt{2\pi}]\eta$.

A^{chain} is expressed as[24,25]

$$\frac{A^{chain}}{NkT} = (1-m)\ln[g^{hs}(d)] \tag{15}$$

where $g^{hs}(d) = 1 - 0.5\eta/(1-\eta)^2$.

The compressibility factor Z can be expressed as

$$Z = \rho\left[\frac{\partial(A/NkT)}{\partial\rho}\right]_{N,T} \tag{16}$$

2.3. Renormalization Group Theory. The fluids become inhomogeneous in the critical region as the long wavelength density fluctuations are important and the correlation between larger and larger numbers of molecules makes an increasingly significant contribution to the Helmholtz free energy. The classical EOS, e.g., the SAFT EOS,[24,25] fails to describe the critical properties because the long-wavelength density fluctuation is ignored. To represent the long-range fluctuations in the critical region, the RGT is employed for the correction of dispersion contribution to the Helmholtz free energy.

For a closed system at temperature T with particle number N and volume V, the canonical partition function is expressed as

$$Q = \frac{1}{N!\Lambda^{3N}}\int e^{-\beta}\Phi\, d\mathbf{r}_1\, d\mathbf{r}_2 \ldots d\mathbf{r}_N \tag{17}$$

where Φ represents total potential energy and $\beta = 1/(kT)$. The partition function itself is exact, near or far from the critical point, provided that the configurational integral is evaluated exactly.

In a standard statistical mechanical approach, the microstates of a classical system are defined by the positions of the individual particles. Naturally, the particle positions appear in the configurational integral. This approach is convenient for discussing fluids far away from the critical point where correlations among particles are dominated by short-ranged repulsion. However, it is not an efficient way to describe critical properties that are characterized by long-ranged correlations.

To describe the role played by long-ranged correlations, a wavelength λ_s that is comparable to the size of a molecule is used to distinguish the short wavelength and long wavelength. Thus, the partition function is rewritten as

$$Q = \sum_{\rho_s(\mathbf{r})} e^{-\beta A[\overline{\rho_s}(\mathbf{r})] - \beta U_s} \tag{18}$$

where $A[\overline{\rho_s}(\mathbf{r})]$ represents the contribution of the Helmholtz energy that is insensitive to density fluctuations with wavelength longer than λ_s, U_s accounts for the remaining contribution, and

$\rho_s(\mathbf{r})$ is the portion of $\rho(\mathbf{r})$ that remains when the density fluctuations with wavelengths $\lambda < \lambda_s$ are omitted.

The essential idea of RGT is that the contributions from the long-wavelength density wave packets can be removed successively from U_s and incorporated into $A[\bar{\rho}_s(\mathbf{r})]$. Subsequently, the set of function summation in the partition function becomes smaller. At the end of this sequence, U_s disappears and an expression for the partition function that includes all levels of fluctuations is obtained.

The contribution to the partition function from density fluctuations with a wavelength longer than λ_s comes primarily from intermolecular attractions. On the mean field approximation level, for a given density function $\rho(\mathbf{r})$, the potential energy due to intermolecular attractions can be written as

$$\Phi = -\frac{1}{2}\int\int d\mathbf{r}\, d\mathbf{r}'\, \rho(\mathbf{r})\, \rho(\mathbf{r}')\, u(|\mathbf{r}-\mathbf{r}'|) \qquad (19)$$

where u is the potential

During the renormalization-group iteration, the partition function remains invariant when the contributions of long-wavelength densities are subtracted from U_s and incorporated into the $A[\bar{\rho}_s(\mathbf{r})]$ term. Suppose that the density wave packets with the wavelength $\lambda_s < \lambda < \lambda_l$ have been subtracted from U_s and incorporated into $A[\bar{\rho}_s(\mathbf{r})]$, the partition function becomes

$$Q = \sum_{\rho_s(\mathbf{r})} \exp\{-\beta \int d\mathbf{r}\, f_s[\bar{\rho}_s(\mathbf{r})] - \beta U_s\} = \sum_{\rho_l(\mathbf{r})} \exp\{-\beta \int dr\, f_l[\bar{\rho}_l(\mathbf{r})] - \beta U_l'\} \qquad (20)$$

where f_s is the free energy density before RG correction and f_l is the free energy density after one RG iteration.

The difference in free energy densities, $\delta f_l[\bar{\rho}_s(\mathbf{r})]$ is defined as

$$\delta f_l[\bar{\rho}_l(\mathbf{r})] = f_l[\bar{\rho}_l(\mathbf{r})] - f_s[\bar{\rho}_s(\mathbf{r})] \qquad (21)$$

can be numerically calculated from

$$e^{-\beta\int d\mathbf{r}\delta f_l[\bar{\rho}_l(\mathbf{r})]} = \sum_{\rho_D(\mathbf{r})} e^{-\beta\int d\mathbf{r}\delta f_D - \beta U_D} \qquad (22)$$

where

$$f_D = f_l[\bar{\rho}_l(\mathbf{r})] - f_s[\bar{\rho}_s(\mathbf{r})] \text{ and } U_D = U_s - U_l \qquad (23)$$

$$\rho_D(\mathbf{r}) = x\cos(\mathbf{k}\cdot\mathbf{r})\ (k_l < k < k_s) \qquad (24)$$

where x is the fluctuation amplitude and $\mathbf{k}$ is the fluctuation wave vector. Equations 21−24 provide the basic recursion equation for the renormalization group theory.

The RG recursion must be performed numerically. A sequence of corrections δf_n, $n = 1, 2, ...$, is added to $f_s(\rho)$ (here $f_s(\rho)$ is the Helmholtz free energy density before RG correction, which can be expressed by classical SAFT EOS) to take into account the contributions of longer wavelength fluctuations. Equations 25−29[11] are used to evaluate δf_n

$$\delta f_n(\rho) = -K_n \ln\frac{\Omega_n^s}{\Omega_n^l}, \quad 0 \le \rho < \rho_{max}/2 \qquad (25)$$

where ρ_{max} is the maximum possible molecule density, $K_n = 1/2^{3n}\beta L^3$, and Ω_n^l and Ω_n^s are the density fluctuations for the long-range attraction and the short-range attraction, respectively

$$\Omega_n^v(\rho) = \int_0^\rho dx\, e^{(-G_n^v(\rho,x)/Kn)}, \quad v = s, l \qquad (26)$$

$$2G_n^v(\rho,x) = \bar{f}_n^v(\rho + x) + \bar{f}_n^v(\rho - x) - 2\,\bar{f}_n^v(\rho), \quad v = s, l \qquad (27)$$

$$\bar{f}_n^l(\rho) = f_{n-1}(\rho) + f_{MF} \qquad (28)$$

$$\bar{f}_n^s(\rho) = f_{n-1}(\rho) + f_{MF}\frac{\psi\bar{\omega}^2}{2^{2n+1}\bar{L}^2}, \quad \left(\bar{L} = \frac{L}{\sigma}\right) \qquad (29)$$

where $f_{MF} = m^2\alpha\rho^2$ is the Helmholtz free energy density obtained by the mean field approximation. L is the initial cutoff length, and ψ is the average gradient of the wavelet function, which can be fitted by the experimental data. α and $\bar{\omega}^2$ are dependent on the potential $u(r)$. For the LJ potential

$$\alpha = -\frac{1}{2}\int u^{LJ}(|\vec{r} - \vec{r}'|)\, d\vec{r} = 5.58\epsilon \qquad (30)$$

$$\bar{\omega}^2 = \frac{1}{3!\alpha\sigma^2}\int r^2 u^{LJ}(|\vec{r} - \vec{r}'|)\, d\vec{r} = 1.27 \qquad (31)$$

3. Results and Discussions

The phase equilibrium requires pressure and chemical potential in both phases to be equal

$$\begin{cases} p^I = p^{II} \\ \mu^I = \mu^{II} \end{cases} \qquad (32)$$

By solving eq 32, the equilibrium density and pressure at temperature T can be obtained simultaneously.

During the RG recursion, because the Helmholtz free energy has no analytical expression, the pressure and chemical potential should be obtained by the numerical method

$$p = \rho^2\left[\frac{\partial(f(\rho)/\rho NkT)}{\partial\rho}\right]_{N,T}kT, \quad \mu = \left[\frac{\partial(f(\rho)/NkT)}{\partial\rho}\right]_{V,T}kT \qquad (33)$$

where $f(\rho)$ is the Helmholtz free energy density that fully includes the contributions of long wavelength fluctuations. At a given temperature, to obtain $f(\rho)$, the iteration procedures, eqs 25−29, are performed five times for each bulk phase.

In the calculations of phase equilibria, there are five adjustable parameters for each fluid: segment number m, soft sphere diameter of each segment σ, dispersion energy parameter of each segment ϵ/k, the average gradient of the wavelet function ψ, and the influence parameter κ. The parameters m, σ, ϵ/k, and κ are obtained by regressing the experimental data of both phase equilibria[40,41] and surface tensions[42,43] below the critical region. The parameter ψ is obtained by fitting to the critical temperature and pressure from experiments.[40,41] L is adopted as 2.0σ according to the work of Jiang and Prausnitz.[11] The regressed parameters are shown in Table 1.

Figures 1−3 present the vapor−liquid coexistence curves and the saturation pressures and $p-\rho$ diagrams in comparison with the experimental data from the literature.[40,41] From the figures, one finds that the SAFT EOS significantly over predicts the critical temperatures as it ignores the long-wavelength density fluctuation. However, by combining the RG correction, the EOS is able to represent both the phase equilibria and critical properties satisfactorily.

TABLE 1: Regressed Parameters for Nonpolar Fluids[a]

	σ, 10^{-10} m	ϵ/k, K	m	ρ^V%	ρ^L%	T range for VLE	T range for γ	γ%	ψ	κ/m^2, J·m^5·mol^{-2}
methane	3.72	147.3	1.00	1.5	0.9	100−155	90−110	1.4	3.0	0.10
ethane	3.48	175.1	1.66	0.6	0.7	150−250	123−183	2.1	4.2	0.23
propane	3.46	181.6	2.21	0.7	0.5	189−296	163−233	2.6	5.8	0.44
butane	3.44	185.2	2.78	1.1	1.1	230−350	230−300	2.7	7.4	0.98
pentane	3.47	193.8	3.17	0.3	0.9	313−413	253−313	2.6	7.5	1.19
hexane	3.50	196.9	3.64	0.4	1.2	283−413	283−373	2.9	8.6	1.77
heptane	3.46	196.9	4.21	0.5	1.6	313−463	283−363	2.5	9.2	2.27
octane	3.46	199.6	4.67	0.7	1.8	320−500	283−383	3.1	9.8	2.84
nonane	3.44	198.3	5.27	0.9	2.3	320−520	423−535	3.4	10.3	3.79
decane	3.25	192.0	6.31	1.5	1.7	447−530	293−540	3.7	12.4	3.86
ARD%				0.9	1.3			2.7		

[a] The experimental data are taken from literature refs 40−43.

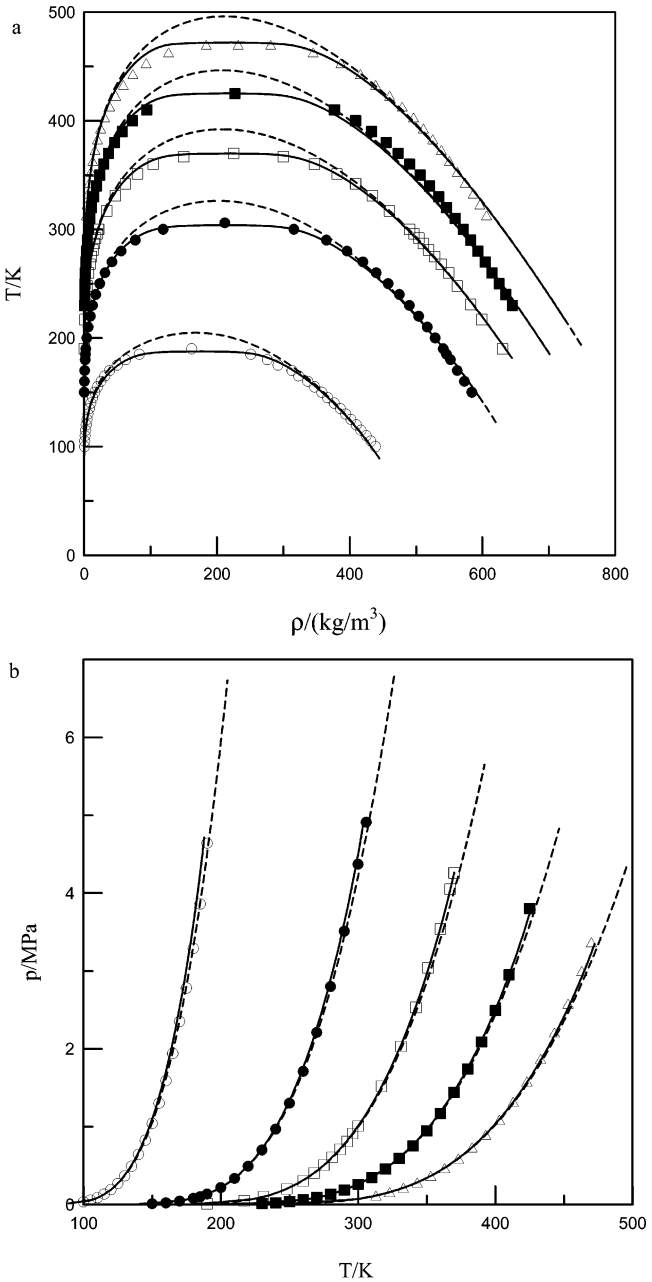

Figure 1. (a) Phase diagrams and (b) the saturation pressures for methane, ethane, propane, butane, and pentane. Symbols: experimental data,[40,41] (○) methane; (●) ethane; (□) propane; (■) butane; (△) pentane. Lines: —, with RG correction; - - -, without RG correction.

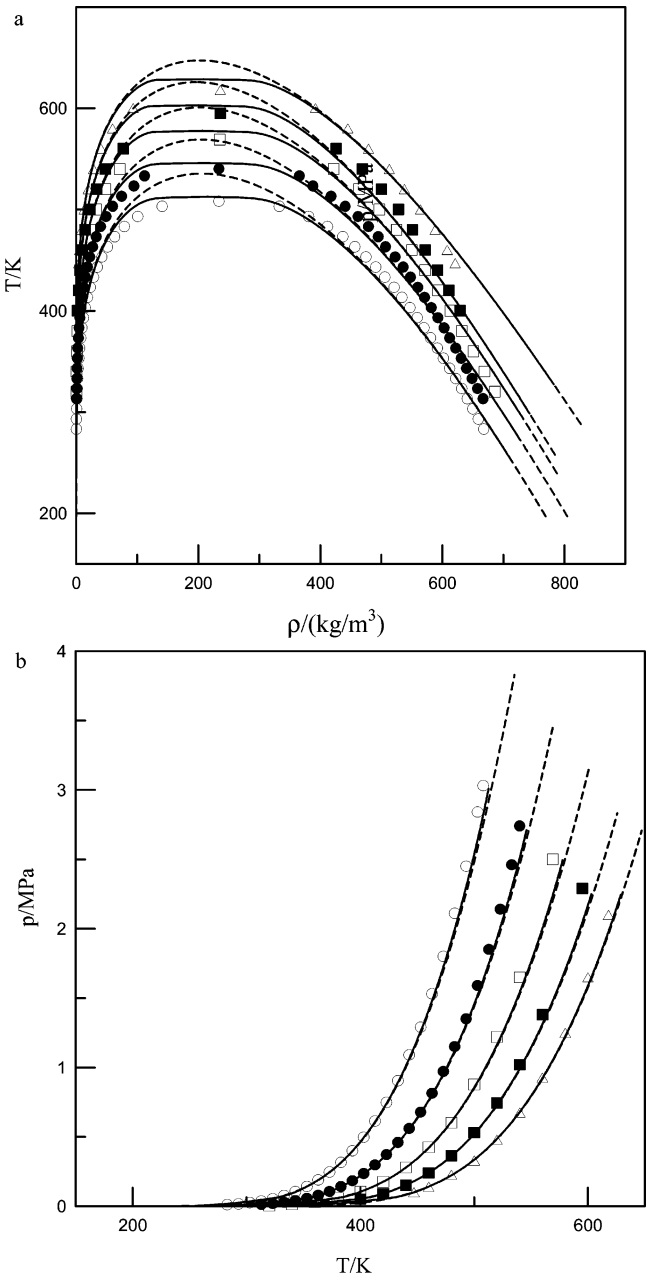

Figure 2. (a) Phase diagrams and (b) the saturation pressures for hexane, heptane, octane, nonane, and decane. Symbols: experimental data,[40,41] (○) hexane; (●) heptane; (□) octane; (■) nonane; (△) decane. Lines: —, with RG correction; - - -, without RG correction.

Table 2 shows the comparison between the critical properties before and after RG correction. One can find that the calculated T_c, p_c, and ρ_c are greatly improved by RG correction. The average relative deviations (ARD%) for T_c, p_c, and ρ_c before

TABLE 2: Comparison between the Calculated Critical Properties and the Experiment Data[a]

	T_c/K			p_c/MPa			ρ_c/kg·m^{-3}		
	exp	cal[1]	cal[2]	exp	cal[1]	cal[2]	exp	cal[1]	cal[2]
methane	190.60	204.86	187.85	4.64	6.73	4.71	162.30	167.02	164.39
ethane	305.50	404.01	304.07	4.91	2.10	4.92	212.18	270.00	215.83
propane	370.00	392.16	370.05	4.27	5.65	4.26	225.00	208.05	223.87
butane	425.20	446.51	425.48	3.80	4.83	3.77	227.01	207.66	228.96
pentane	469.80	496.12	472.27	3.37	4.36	3.35	231.50	211.02	231.11
hexane	507.85	535.41	510.63	3.03	3.83	3.01	234.40	206.05	229.01
heptane	539.71	569.01	543.99	2.74	3.45	2.71	234.10	203.96	230.47
octane	569.40	600.68	574.72	2.50	3.15	2.49	234.74	201.71	229.41
nonane	594.60	625.79	600.97	2.29	2.83	2.25	236.41	196.26	229.33
decane	617.60	647.25	625.75	2.10	2.71	2.24	235.90	202.26	231.04
ARD%		8.3	0.7		33.2	1.4		12.5	1.6

[a] The experimental data are taken from literature refs 40 and 41. The superscripts 1 and 2 stand for the results without and with RG correction, respectively.

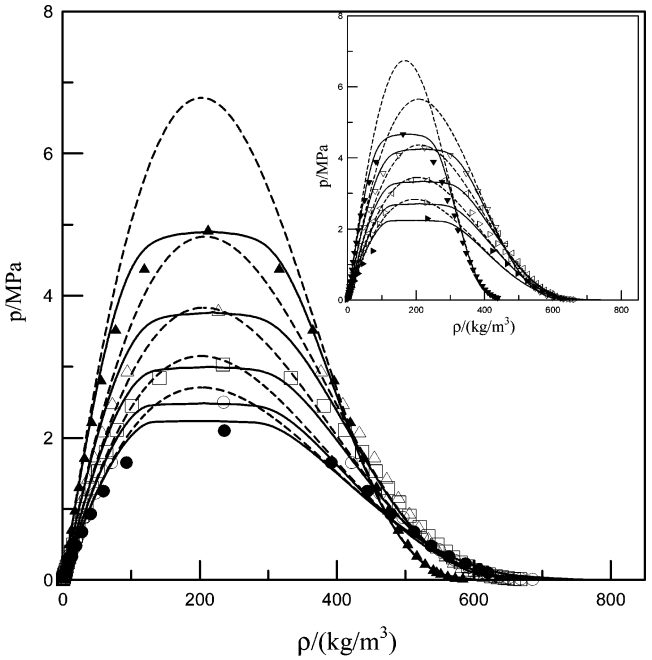

Figure 3. Pressure−density coexistence curves for *n*-alkanes. Symbols: experimental data,[40,41] (▼) methane; (▽) propane; (open left-facing triangle) pentane; (open right-facing triangle) heptane; (solid right-facing triangle) nonane; (▲) ethane; (△) butane; (□) hexane; (○) octane; (●) decane. Lines: —, with RG correction; - - -, without RG correction.

the RG correction are 8.3%, 33.2%, and 12.5%, respectively, whereas after RG correction they become 0.7%, 1.4%, and 1.6%, correspondingly.

It is worth noting that the used molecular parameters may not yield the best results for phase equilibria and critical properties. As shown in Figures 2 and 3, the deviation of the calculated coexistence curve from the experimental data in the critical region increases as the molecular weight increases. Moreover, although the calculated critical exponents [$\beta = 0.327$ from the power law $(\rho^L - \rho^V)/\rho_c = 2B(1 - T/T_c)^\beta$] for alkanes from methane to octane are very close to the experimental nonclassical critical exponent, those for nonane and decane ($\beta = 0.321$ and 0.317, respectively) deviate the experimental data significantly. The deviations can be explained by the fact that the molecular parameters are regressed from the experimental data of both phase equilibria and surface tensions so that the surface tensions for each alkane can be well described by using a unique influence parameter κ.

For vapor−liquid surface, to determine the equilibrium density profile $\rho(z)$ at a given temperature, 1000 densities ($\rho_i = \rho^V + i(\rho^L - \rho^V)/999$, $i = 0,999$) are preset across the surface.

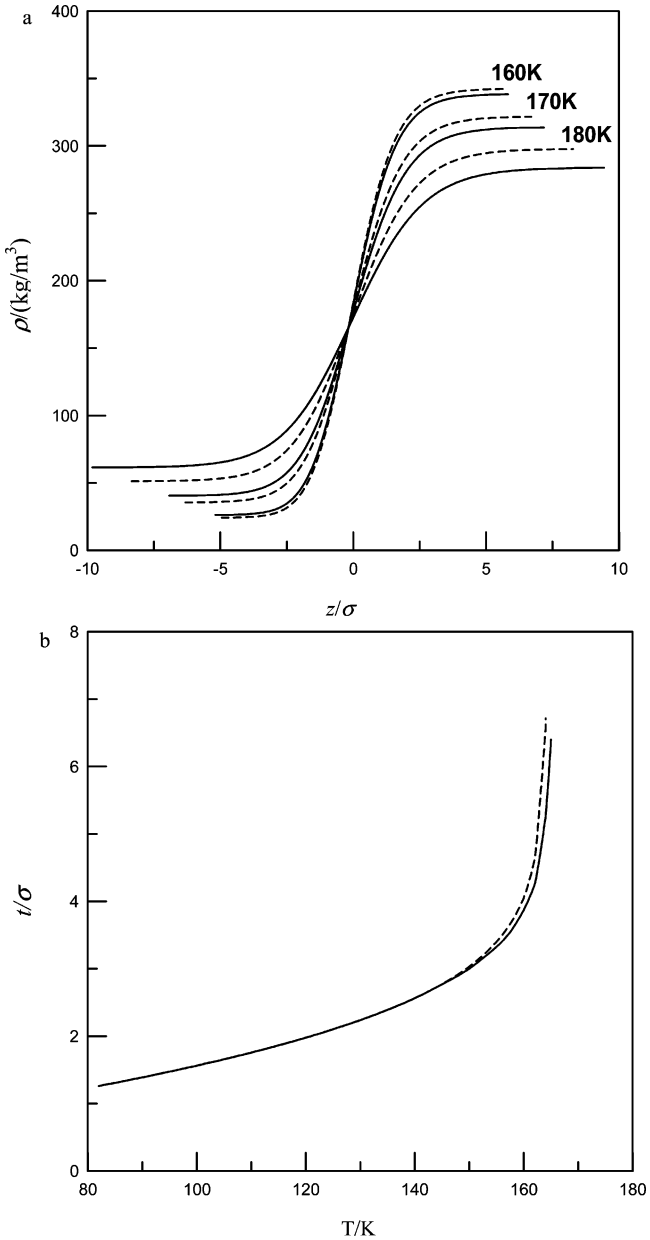

Figure 4. Density profile and surface thickness for methane predicted by DGT (—, with RG correction; - - -, without RG correction).

For each ρ_i, the corresponding Helmholtz free energy density and chemical potential which fully include the contributions of long wavelength fluctuations can be obtained by using the RG correction; hence, $\rho(z)$ can be calculated from eq 6.

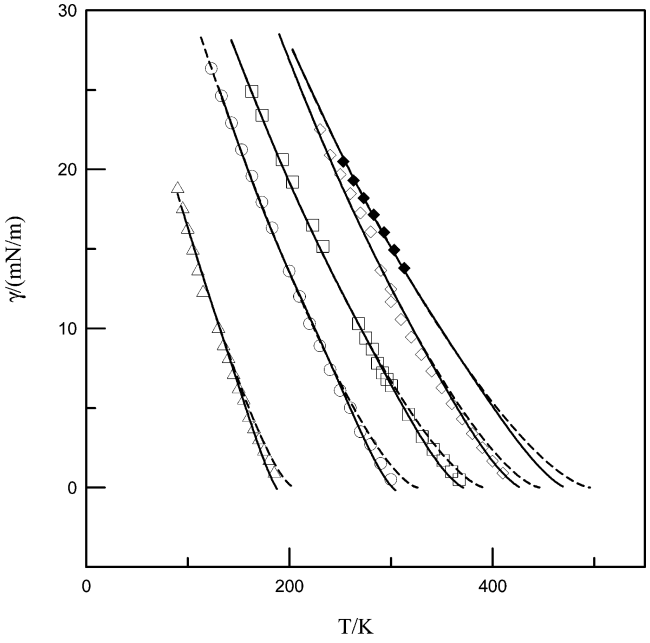

Figure 5. Surface tensions for (△) methane; (○) ethane; (□) propane; (◇) butane; (▼) pentane. Symbols: experimental data.[42,43] Lines: —, predicted with RG correction; - - -, predicted without RG correction.

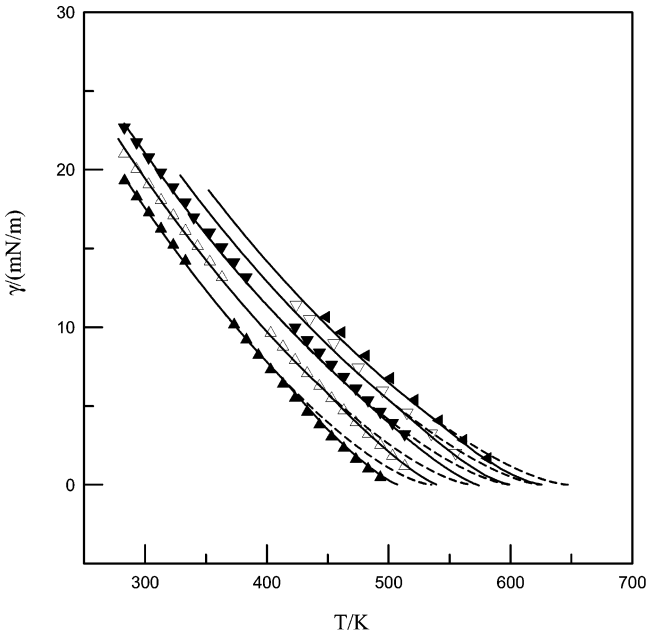

Figure 6. Surface tensions for (▲) hexane; (△) heptane; (▼) octane; (▽) nonane; (solid left-facing triangle) decane. Symbols: experimental data.[42,43] Lines: —, predicted with RG correction; - - -, predicted without RG correction.

Figure 4 presents the interfacial density profile and surface thickness (t) for methane. Figure 4a compares the density profiles obtained with and without RG correction, showing that both methods yield smooth density profiles. In the low temperature region, density profiles obtained by these two methods are similar, whereas inside the critical region, the classical EOS broadens the vapor−liquid surface as it under estimates the vapor density and over estimates the liquid density. Figure 4b compares the surface thickness obtained by the 10−90% rule[44] with and without RG correction. Besides the basic feature that the calculated surface thickness is several times of the soft-sphere diameter and increases with temperature, Figure 4b shows that the classical EOS over estimates the surface thickness in the critical region. Figures 5 and 6 present the surface tensions for 10 nonpolar fluids predicted by DGT. From these two figures, one can find that by regressing the influence parameter with experimental data of surface tensions, DGT gives satisfactory results for surface tensions below the critical region. Inside the critical region, the classical EOS over predicts the surface tensions due to the overestimation of the critical temperature. However, after RG correction, DGT correctly predicts the surface tensions inside the critical region, and the results agree well with the experimental data.

4. Conclusions

The phase equilibria and interfacial properties for 10 nonpolar fluids are investigated by using DGT and RGT. The results show the following:

(1) Both the phase equilibria and surface tensions below the critical region can be fitted well by using DGT and SAFT EOS. The average relative deviations for liquid density ρ^L, vapor pressure p^V, and surface tension γ are 1.3%, 0.9%, and 2.7%, respectively.

(2) Using the obtained parameters, SAFT EOS and DGT over predict the phase equilibria and surface tensions inside the critical region. However, by combining SAFT EOS and DGT with the RGT, both the bulk and interfacial properties inside the critical region can be satisfactorily predicted.

Acknowledgment. The author appreciates the financial support from the National Natural Science Foundation of China (Grant No. 20576030) and the key program foundation from NCEPU.

References and Notes

(1) Evans, R. *Adv. Phys.* **1979**, *28*, 143.
(2) Evans, R. Density functionals in the theory of nonuniform fluids. In *Fundamentals of Inhomogeneous Fluids*; Henderson, D., Ed.; Marcel Dekker: New York, 1992.
(3) Davis, H. T. *Statistical mechanics of phases, interfaces and thin films*; VCH: New York, 1996.
(4) Wilson, K. G. *Phys. Rev. B* **1971**, *4*, 3184.
(5) White, J. A.; Zhang, S. *J. Chem. Phys.* **1995**, *103*, 1922.
(6) White, J. A.; Zhang, S. *Int. J. Thermophys.* **1998**, *19*, 1019.
(7) White, J. A. *J. Chem. Phys.* **2000**, *112*, 3236.
(8) White, J. A. *J. Chem. Phys.* **2000**, *113*, 1580.
(9) Lue, L.; Prausnitz, J. M. *J. Chem. Phys.* **1998**, *108*, 5529.
(10) Lue, L.; Prausnitz, J. M. *AIChE J.* **1998**, *44*, 1455.
(11) Jiang, J. W.; Prausnitz, J. M. *J. Chem. Phys.* **1999**, *111*, 5964.
(12) Fu, D.; Li, Y. G.; Wu, J. Z. *Phys. Rev. E* **2003**, *68*, 011403.
(13) Fu, D.; Li, Y. G. *Ind. Eng. Chem. Res.* **2004**, *43*, 2271.
(14) Fu, D.; Zhao, Y.; Li, Y. G. *Ind. Eng. Chem. Res.* **2004**, *43*, 5425.
(15) Mi, J. G.; Zhong, C. L.; Li, Y. G.; Tang, Y. P. *J. Chem. Phys.* **2004**, *121*, 5372.
(16) Kiselev, S. B. *Fluid Phase Equilib.* **1998**, *147*, 7.
(17) Kiselev, S. B.; Ely, J. F. *Ind. Eng. Chem. Res.* **1999**, *38*, 4993.
(18) Kiselev, S. B.; Ely, J. F.; Adidharma, H.; Radosz, M. *Fluid Phase Equilib.* **2001**, *183*−*184*, 53.
(19) Kiselev, S. B.; Ely, J. F.; Lue, L.; Elliott, Jr. *Fluid Phase Equilib.* **2002**, *200*, 121.
(20) Kiselev, S. B.; Ely, J. F. *J. Chem. Phys.* **2003**, *119*, 8645.
(21) Kiselev, S. B.; Ely, J. F. *Fluid Phase Equilib.* **2004**, *222*−*223*, 149.
(22) Sun, L. X.; Kiselev, S. B.; Ely, J. F. *Fluid Phase Equilib.* **2005**, *233*, 204.
(23) Kiselev, S. B.; Ely, J. F.; Tan, S. P.; Adidharma, H.; Radosz, M. *Ind. Eng. Chem. Res.* **2006**, *45*, 3981.
(24) Chapman, W. G.; Gubbins, K. E.; Jackson, G.; Radosz, M. *Fluid Phase Equilib.* **1989**, *52*, 31.
(25) Huang, S. H.; Radosz, M. *Ind. Eng. Chem. Res.* 1990, *29*, 2284.
(26) Rosenfeld, Y. *J. Chem. Phys.* **1993**, *98*, 8126.
(27) Wadewitz, T.; Winkelmann, J. *J. Chem. Phys.* **2000**, *13*, 2447.
(28) Oxtoby, D. W. *Annu. Rev. Mater. Res.* **2002**, *32*, 39.
(29) Yu, Y. X.; Wu, J. Z. *J. Chem. Phys.* **2002**, *117*, 10156.
(30) Tang, Y. P.; Wu, J. Z. *J. Chem. Phys.* **2003**, *109*, 7388.
(31) Fu, D.; Wu, J. *Mol. Phys.* **2004**, *102*, 1479.
(32) Fu, D. *J. Chem. Phys.* **2006**, *124*, 164701.

(33) Cahn, J. W.; Hilliard, J. E. *J. Chem. Phys.* **1958**, *28*, 258.
(34) Cornelisse, P. M. W.; Peters, C. J.; Arons, J. S. *Mol. Phys.* **1993**, *80*, 941.
(35) Cornelisse, P. M. W.; Peters, C. J.; Arons, J. S. *Fluid Phase Equilib.* **1993**, *82*, 119.
(36) Cornelisse, P. M. W.; Peters, C. J.; de Swaan Arons, J. *J. Chem. Phys.* **1997**, *106*, 9820.
(37) Zuo, Y. X.; Stenby, E. H. *J. Colloid Interface Sci.* **1996**, *182*, 126.
(38) Carnahan, N. F.; Starling, K. E. *J. Chem. Phys.* **1969**, *51*, 635.
(39) Cotterman, R. L.; Schwarz, B. J.; Prausnitz, J. M. *AIChE J.* **1986**, *32*, 1787.
(40) Beaton, C. F.; Hewitt, G. F. *Physical property data for the design engineer*; Hemisphere Publishing Corporation: New York, 1989.
(41) Smith, B. D.; Srivastava, R. *Thermodynamic data for pure components*; Elsevier: Amsterdam, 1986.
(42) Jasper, J. J. *J. Phys. Chem. Ref. Data* **1972**, *1*, 841.
(43) Vargaftik, N. B. *Tables on the thermo-physical properties of liquids and gases*; Hemisphere Publishing Corporation: New York, 1975.
(44) Rowlinson, J. S.; Widom, B. *Molecular theory of capillarity*; Clarendon Press: Oxford, 1982.